

# THERMAL EMISSION FROM THE DUST COMA OF COMET HALE-BOPP AND THE COMPOSITION OF THE SILICATE GRAINS

M.S. Hanner<sup>1</sup>, R.D. Gehrz<sup>2</sup>, D.E. Harker<sup>3</sup>, T.L. Hayward<sup>4</sup>, D.K. Lynch<sup>5</sup>, C.C. Mason<sup>2</sup>, R.W. Russell<sup>5</sup>, D.M. Williams<sup>2</sup>, D.H. Wooden<sup>6</sup>, and C.E. Woodward<sup>3</sup>

<sup>1</sup>*MS 183-501 Jet Propulsion Laboratory, California Institute of Technology, Pasadena CA 91109 USA*

<sup>2</sup>*Astronomy Dept., Univ. Minnesota, Minneapolis MN 55455 USA*

<sup>3</sup>*Wyoming Infrared Observatory, Physics & Astronomy Dept., Univ. Wyoming, Laramie WY 82071 USA*

<sup>4</sup>*Astronomy Dept. Cornell University, Ithaca NY 14853 USA*

<sup>5</sup>*Aerospace Corp., M2-266, P.O. Box 92957, Los Angeles CA 90009-2957 USA*

<sup>6</sup>*MS 245-6 NASA Ames Research Center, Moffett Field CA 94035-1000 USA*

**Abstract.** The dust coma of comet Hale-Bopp was observed in the thermal infrared over a wide range in solar heating ( $R=4.9-0.9$  AU) and over the full wavelength range from  $3\text{ }\mu\text{m}$  to  $160\text{ }\mu\text{m}$ . Unusual early activity produced an extensive coma containing small warm refractory grains; already at  $4.9$  AU, the  $10\text{ }\mu\text{m}$  silicate emission feature was strong and the color temperature was  $\sim 30\%$  above the equilibrium blackbody temperature. Near perihelion the high color temperature, strong silicate feature, and high albedo indicated a smaller mean grain size than in other comets. The  $8-13\text{ }\mu\text{m}$  spectra revealed a silicate emission feature similar in shape to that seen in P/Halley and several new and long period comets. Detailed spectral structure in the feature was consistent over time and with different instruments; the main peaks occur at  $9.3$ ,  $10.0$  and  $11.2\text{ }\mu\text{m}$ . These peaks can be identified with olivine and pyroxene minerals, linking the comet dust to the anhydrous chondritic aggregate interplanetary dust particles. Spectra at  $16-40\text{ }\mu\text{m}$  taken with the ISO SWS displayed pronounced emission peaks due to Mg-rich crystalline olivine, consistent with the  $11.2\text{ }\mu\text{m}$  peak.

**Key words:** comet Hale-Bopp, infrared, dust, silicates

## 1. Introduction

The early discovery of Comet Hale-Bopp and its strong activity at large heliocentric distance provided a rare opportunity to observe the dust over a wide range in solar heating. Even beyond  $4$  AU, where the blackbody temperature was  $< 140$  K, surprisingly strong thermal emission indicated an extensive dust coma of small refractory (silicate and absorbing) grains. This strong thermal emission persisted throughout the comet's apparition.

There has been a revolution in infrared detector technology in the past decade that was just beginning at the time of comet P/Halley (Hanner & Tokunaga 1991). Sensitive 1- and 2- dimensional arrays are now common in the near- and mid-infrared and Hale-Bopp is the first bright comet for which we could take full advantage of these new instruments. Moreover, Hale-Bopp was also observed from ESA's Infrared Space Observatory (ISO), considerably extending the wavelength coverage for both photometry and spectroscopy.

Three types of infrared observations contribute to our knowledge of dust properties. Photometry, the measure of total flux versus wavelength, defines the spectral energy distribution; imaging displays the spatial structures of the dust coma; and low-resolution spectroscopy, particularly in the region of the 10 and 20  $\mu\text{m}$  silicate features, gives information about the composition and mineralogy of the grains. We define the thermal infrared as the spectral region between about 3  $\mu\text{m}$ , where the thermal emission begins to dominate over the scattered light, and 200  $\mu\text{m}$ , the long wavelength limit for ISO. The near-infrared, from 1 - 2.5  $\mu\text{m}$ , provides complementary measurements of the dust albedo, color and polarization.

In this paper, we focus on the mid-infrared photometry and spectroscopy of the dust during 1996 and 1997 and discuss the dust composition and size. It has long been a puzzle how cometary dust relates to the interplanetary dust particles (IDPs) captured in the stratosphere and subjected to intensive laboratory analysis. The high signal/noise spectra of Hale-Bopp at last provide a convincing link to the chondritic aggregate IDPs.

## 2. Thermal Spectral Energy Distribution

The thermal radiation from a single grain depends on its temperature and wavelength-dependent emissivity.

$$F_{\lambda} = \frac{a^2}{\Delta^2} \varepsilon(\lambda, a) \pi B_{\lambda}(T(a)) \quad (1)$$

where  $\varepsilon(\lambda, a)$  is the grain emissivity,  $a$  is the grain radius  $\Delta$  is the geocentric distance, and  $B(\lambda, T)$  is the Planck function for grain temperature  $T$ . Because of  $\varepsilon(\lambda, a)$ , the observed spectral energy distribution from a single grain will not follow that of a simple blackbody.

The temperature of a grain in the coma is determined by the balance between solar energy absorbed at visual wavelengths and the energy

emitted in the infrared. Here we assume that the coma is optically thin (no heating by other grains) and that sublimation is negligible.

$$\frac{\pi a^2}{r^2} \int_0^\infty S(\lambda) Q_{abs}(\lambda, a) d\lambda = 4\pi a^2 \int_0^\infty Q_{abs}(\lambda, a) \pi B_\lambda(T(a)) d\lambda \quad (2)$$

where  $S$  is the solar flux at 1 AU and  $r$  is the heliocentric distance in AU.

Small carbonaceous grains absorb strongly at visual wavelengths, but cannot radiate efficiently at infrared wavelengths more than  $\sim 10$  times their size. Thus, they heat up until the energy radiated at 3-8  $\mu\text{m}$  balances the absorbed energy. In fact, for small featureless absorbing grains, their size controls their temperature, regardless of the specific optical constants (Hanner 1983). It can be seen in Fig. 1 that grains smaller than  $\sim 1 \mu\text{m}$  radius will be hotter than a theoretical blackbody. Grains larger than a few microns will be warmer than a blackbody only if they are very fluffy and the unit structure is micron-sized or smaller (Xing & Hanner 1997; Greenberg & Hage 1990).

In contrast to small carbon grains, small silicate grains radiate efficiently in the infrared; it is the amount of absorption at visual wavelengths that controls their temperature. Fig. 2 plots  $T(r)$  for silicate grains of radius 0.5  $\mu\text{m}$  and differing imaginary index of refraction at visual wavelengths,  $k$ . Mg-rich silicates have low absorption ( $k < 0.001$ ; Dorschner et al. 1995), and consequently will be much cooler than a blackbody. For glassy silicate with Fe/Mg  $\sim 0.5$ ,  $k \sim 0.01$  and the temperature of a 0.5  $\mu\text{m}$  radius grain will be close to that of a blackbody. For olivine glass with Fe/Mg  $\sim 1$ ,  $k \sim 0.1$  (Dorschner et al.) and the temperature of a sub-micron sized grain will be quite hot, hotter even than a carbon grain. Small silicate grains can also be heated if they have carbonaceous material adhering to them (core-mantle grains, aggregates, etc.).

The absorptivity, hence temperature, for organic residue grains depends on the ratio of C/H and can vary from  $k \sim 0.01$  to 0.1 or more (Khare et al. 1984). Consequently, small organic residue grains can have temperatures comparable to a blackbody ( $k \sim 0.01$  in Fig. 2) or somewhat hotter.

The thermal emission actually observed at a given wavelength will be the sum total of the emission from grains of all sizes, compositions, and temperatures along the line of sight. The observed color temperature,  $T_c$ , will be the envelope of emission from all grains and will not be equal to the actual temperature of the grains. Since smaller, warmer grains will emit more strongly at shorter wavelengths,  $T_c$  can

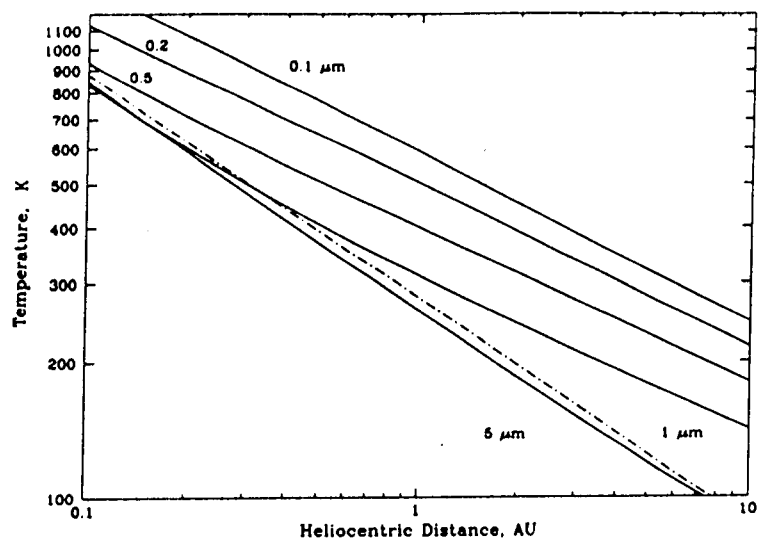


Figure 1. Grain temperature versus heliocentric distance for glassy carbon spheres with radius 0.1, 0.2, 0.5, 1.0, and 5.0  $\mu\text{m}$ . Dashed-dot line is the equilibrium blackbody temperature.

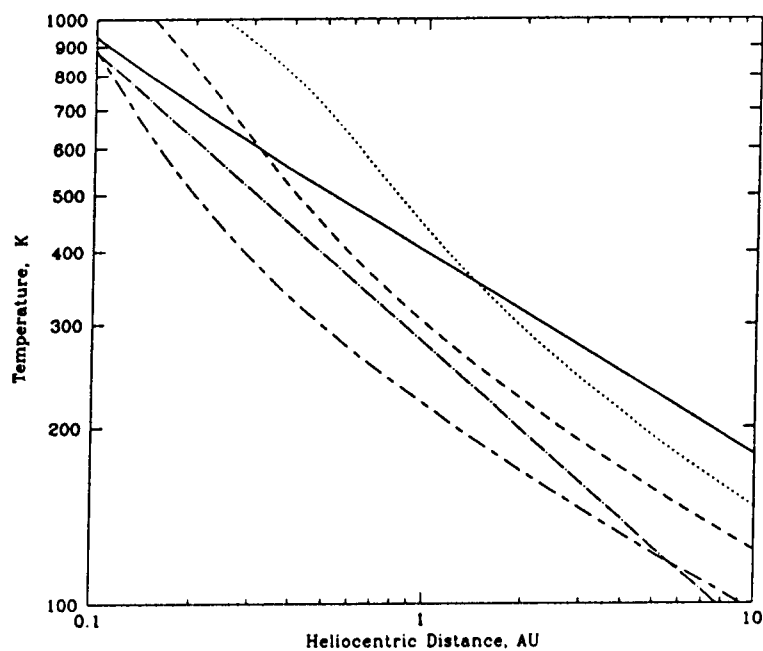


Figure 2. Grain temperature versus heliocentric distance for 0.5  $\mu\text{m}$  radius silicate spheres with refractive index at visual wavelengths  $n=1.69-ik$ . Short-long dashes— — —  $k=0.001$ ; ---  $k=0.01$ ; ..... Fe olivine with  $\text{Fe}/\text{Mg} = 1$  (Dorschner et al. 1995); \_\_\_\_\_ glassy carbon; ----  $T_{\text{BB}}$ .

vary with wavelength.

The earliest mid-infrared spectral energy distribution of Hale-Bopp, displayed in Fig. 3, was acquired with the ISO PHOT-S spectrometer on 27 April 1996 at  $r=4.6$  AU (Crovisier et al. 1996). Strong excess emission is visible from  $\sim 8 \mu\text{m}$  to the  $11.5 \mu\text{m}$  limit of the ISOPHOT spectrum. This feature is very similar to that produced by small silicate grains and seen in a number of comets at smaller  $r$ . This strong feature was a surprise; we had expected a coma of colder icy grains at such large  $r$ , similar to the icy grain halo in comet Bowell at  $r > 4$  AU. The Planck function fit to the  $6 - 8 \mu\text{m}$  continuum corresponds to  $T_c=162$  K, 25% hotter than the blackbody temperature of 130 K at 4.6 AU and indicative of small grains containing at least some absorbing material.

Photometry of Hale-Bopp through broad filters from  $3.6$  to  $160 \mu\text{m}$  was obtained with the ISOPHOT photometers at 4.92, 4.6, 2.9, and 2.8 AU and at 3.9 AU postperihelion (Grün et al. 1998; Peschke et al. 1998). These data are consistent with Fig. 3 in showing thermal emission from warm grains and strong excess emission at  $10 \mu\text{m}$ . Detection of dust continuum emission at 100 and  $164 \mu\text{m}$  demonstrates that large grains, radius  $> 10 \mu\text{m}$ , were present in the coma as well. Cold icy grains may also contribute to the long-wavelength emission.

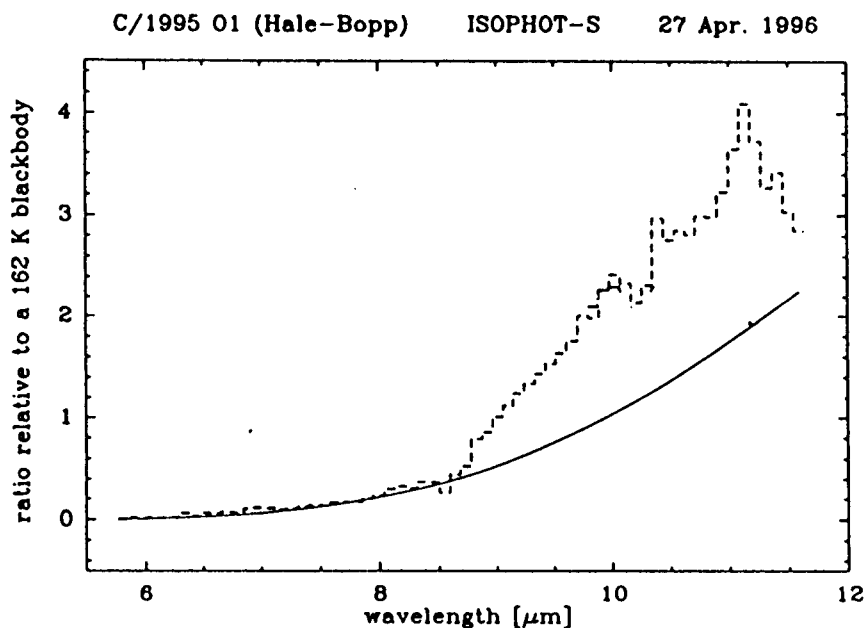


Figure 3. 6-11.5  $\mu\text{m}$  spectrum of Hale-Bopp at  $R=4.6$  AU, taken with the ISO PHOT-S instrument and a  $24'' \times 24''$  field of view. Solid line is a 162 K blackbody fitted at 6-8  $\mu\text{m}$  (Crovisier et al. 1996).

Absorption features of water ice at 1.5 and 2.05  $\mu\text{m}$  were detected by Davies et al. (1997) when the comet was at  $r = 7$  AU; at that time, icy grains must have been abundant in the coma. However, Davies et al. (1998) failed to detect these features at 4.6 AU against the stronger scattered light from the coma. Any ice mixed with grains at  $T \sim 160$  K near 4.6 AU would have sublimated rapidly.

Thus, at 4.6 AU, the dust coma of Hale-Bopp was very different from the inferred coma of comet Bowell at similar  $r$ . The high OH production observed for comet Bowell at  $r > 4$  AU led A'Hearn et al. (1984) to propose that the sublimation arose from large icy grains. Hanner & Campins (1986) showed that the total mid-infrared flux from the coma could be produced from these icy grains at  $T \sim 150$  K; a population of small dark grains was not necessary to explain the thermal emission. At 3.5 AU, Hale-Bopp was about 45 times as bright at 10  $\mu\text{m}$  as Bowell at 3.5 AU.

The 1 - 20  $\mu\text{m}$  spectral energy distribution (SED) was measured on 13 dates between 20 Feb and 11 June 1997 at O'Brien Observatory (U. Minn.) or Mt. Lemmon. An example of the SED at  $r=1.15$  AU pre-perihelion is shown in Fig. 4 (Williams et al. 1997). Scattered light, approximating the solar SED, is evident at 1 - 2.2  $\mu\text{m}$ ; it is stronger relative to the thermal emission than most comets near 1 AU. The high flux at 3.6 - 5  $\mu\text{m}$  and the 475 K color temperature, higher relative to a blackbody than in any other comet observed to date, are clear signatures of small absorbing grains a few 0.1  $\mu\text{m}$  in size (Fig. 1 & 2). The wavelength dependence of  $T_c$  is evident; the 475 K Planck function falls well below the continuum at 8 and 12.5  $\mu\text{m}$ . Strong silicate emission generally correlates with a high  $T_c$  (e.g. Gehrz & Ney 1992) and Hale-Bopp clearly fits this pattern. Either the abundance of small carbonaceous grains correlates with the abundance of small silicate grains or the silicate grains are very Fe-rich and therefore hot, contradicting the spectral evidence for high Mg content.

An albedo  $A(\theta)$  can be defined at the scattering angle of observation by the relation given in Williams et al. (1997)

$$\frac{A(\theta)}{1 - A(\theta)} = \frac{(\lambda F_\lambda(\theta))_{\text{max. vis}}}{(\lambda F_\lambda(\theta))_{\text{max. ir}}} \quad (3)$$

Fig. 5 compares the albedo  $A(\theta)$  for Hale-Bopp, based on this data set, with P/Halley and other comets observed by Gehrz & Ney (1992). The grains in Hale-Bopp were twice as bright as those in other comets near  $\theta = 140$  deg; the rise towards backscatter at  $\theta > 150$  deg is typical of other comets, including P/Halley (Millis et al. 1982; Tokunaga et al.

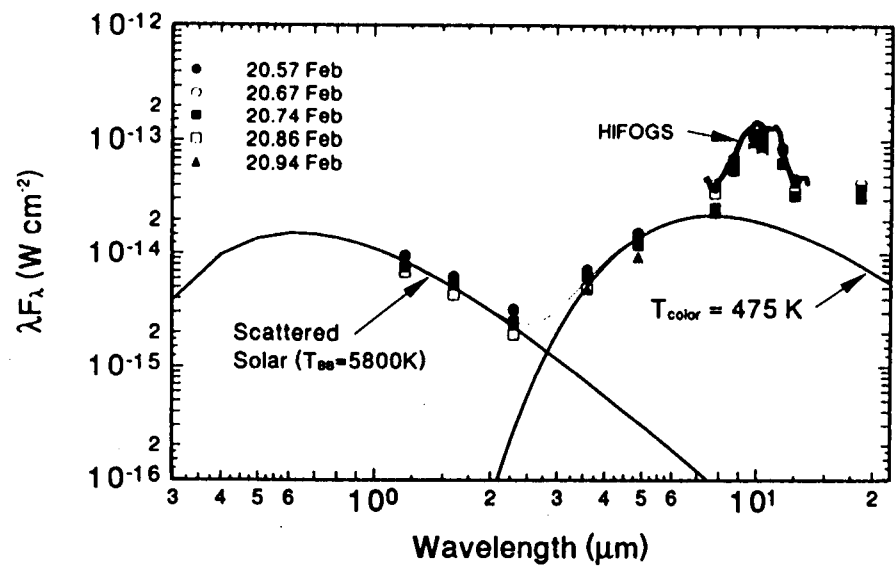


Figure 4. Infrared spectral energy distribution of Hale-Bopp at  $r=1.15$  AU (Williams et al. 1997).

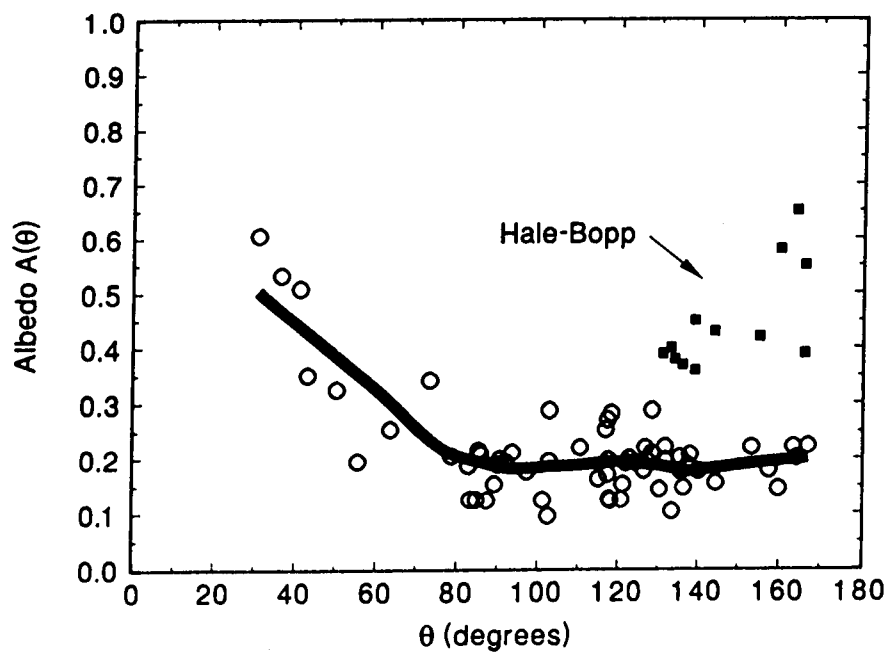


Figure 5. Albedo  $A(\theta)$  versus scattering angle  $\theta$  for Hale-Bopp (squares) and comets measured by Gehrz & Ney (1992) (circles).

1986). The higher  $A(\theta)$  may be due to the smaller mean grain size and/or to a higher abundance of silicate grains relative to carbonaceous grains in Hale-Bopp.

The infrared flux dropped by a factor  $\sim 3$  a few weeks after perihelion and the comet remained fainter in the infrared postperihelion than at similar distances preperihelion (Wooden et al. 1997; Galdemard et al. 1998).

### 3. The Silicate Features

#### 3.1 THE OBSERVED SPECTRA

Small silicate grains produce a spectral feature near  $10\ \mu\text{m}$  due to stretching vibrations in Si-O bonds, within the  $8\text{--}13\ \mu\text{m}$  atmospheric window available to groundbased observations. The spectral shape of the feature can be diagnostic of the silicate mineralogy. A review of the  $10\ \mu\text{m}$  spectra of comets is given by Hanner et al. (1994). Additional spectral bands occur at longer wavelengths, fully accessible only from above the earth's atmosphere.

Hale-Bopp already displayed strong  $10\ \mu\text{m}$  emission at 4.9 AU (Peschke et al. 1998). The development of the silicate feature in 1996-1997 was monitored primarily with three instruments. The Aerospace Corp. broad-band array spectrograph (BASS) was used at the 3-m NASA Infrared Telescope Facility (IRTF) and Mt. Lemmon (Russell et al. 1997). It spans the wavelength region  $2\text{--}14\ \mu\text{m}$  using two 58-element blocked impurity band linear arrays (Hackwell et al. 1990). All spectral elements are observed simultaneously; there are no moving parts. Spectral resolution,  $R = \lambda/(\Delta\lambda)$ , is about 70 at  $10\ \mu\text{m}$ . SpectroCam-10 (SC10), a mid-infrared imaging spectrograph with a  $128 \times 128$  element array, was used on the 5-m Hale telescope at Palomar Observatory (Hayward & Hanner 1997, 1998). In the spectral mode, a  $1 \times 16$  arcsec slit was employed, giving  $R \sim 100$  at  $10\ \mu\text{m}$ . The NASA HIFOGS spectrometer was used at the IRTF and the 2.3-m Wyoming Infrared Observatory (Wooden et al. 1998a, b). The 120 Si:Bi detectors observe the  $7.5\text{--}13.5\ \mu\text{m}$  region simultaneously with  $R \sim 220$  at  $10\ \mu\text{m}$ . Additional spectra were obtained with the ISO SWS spectrometer (Crovisier et al. 1997), the UKIRT CGS3 spectrometer (Davies et al. 1998) and with a circular variable filter ( $R \sim 50$ ) at the 2.6m Nordic Optical Telescope in April 1997 (Galdemard et al. 1998).

The development of the spectrum from 4.1 AU to 0.92 AU is displayed in Fig. 6. Each spectrum has been divided by a blackbody

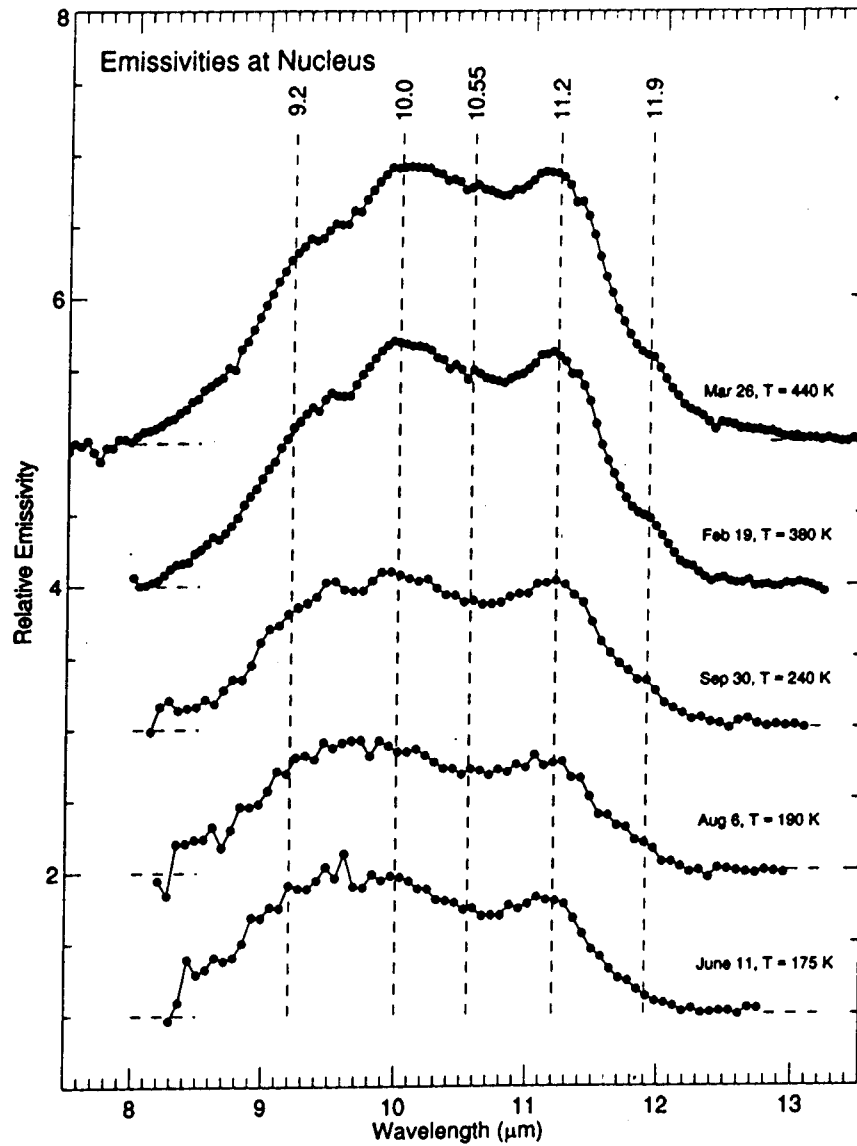


*Figure 6.* Development of the silicate feature in Hale-Bopp from 4.1 – 0.92 AU. Spectra taken with SpectroCam 10 (Hayward & Hanner 1998). Each spectrum has been divided by a blackbody curve for the temperature given in the label and shifted upwards by an amount indicated by the dashed baseline.

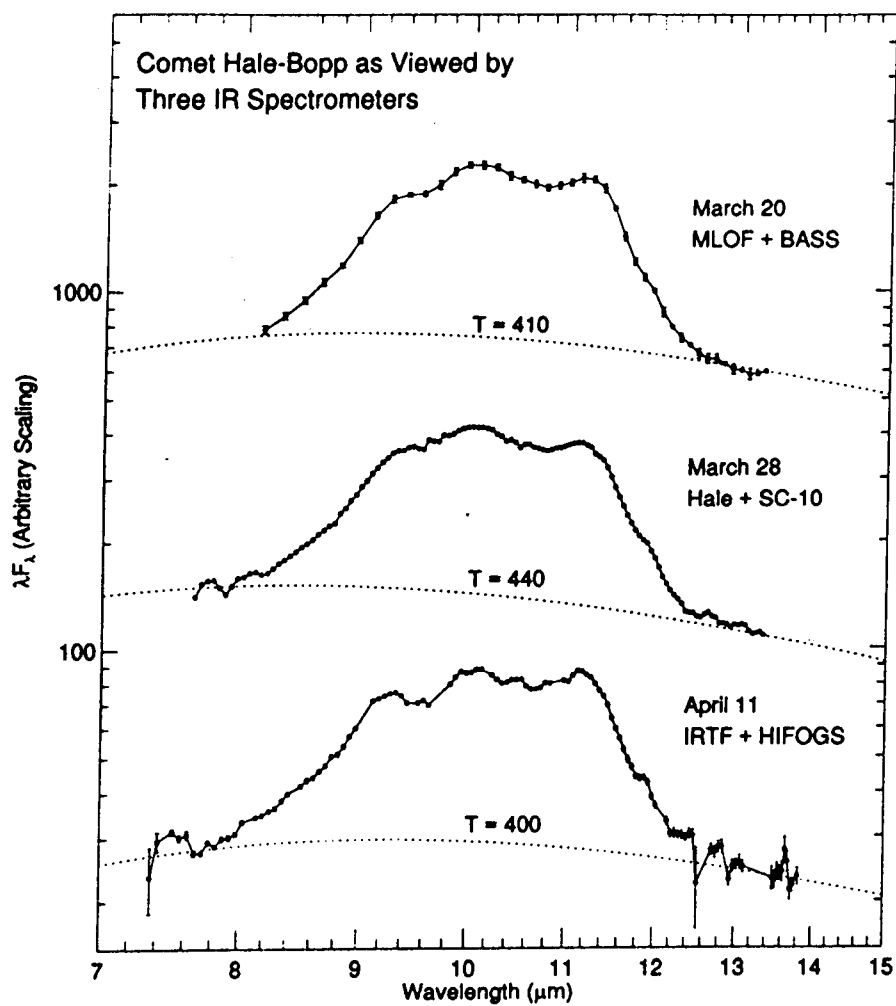


Figure 7. The silicate features in Hale-Bopp as viewed by 3 different spectrometers (see text).

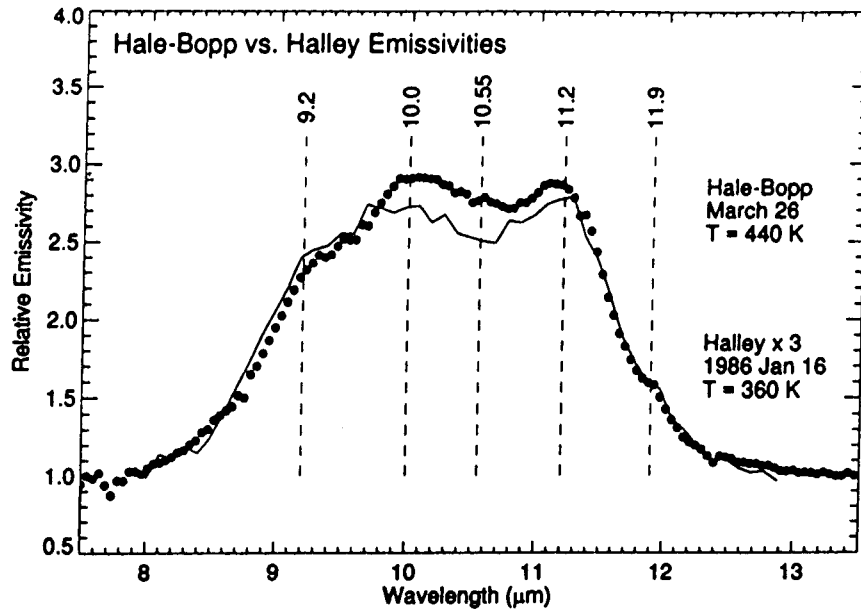


Figure 8. Comparison of the silicate feature in Hale-Bopp (points) and Halley (solid line). Halley spectrum is from Campins & Ryan (1989). Each spectrum has been divided by a blackbody for the temperature shown in the label and the Halley spectrum has been multiplied by 3.

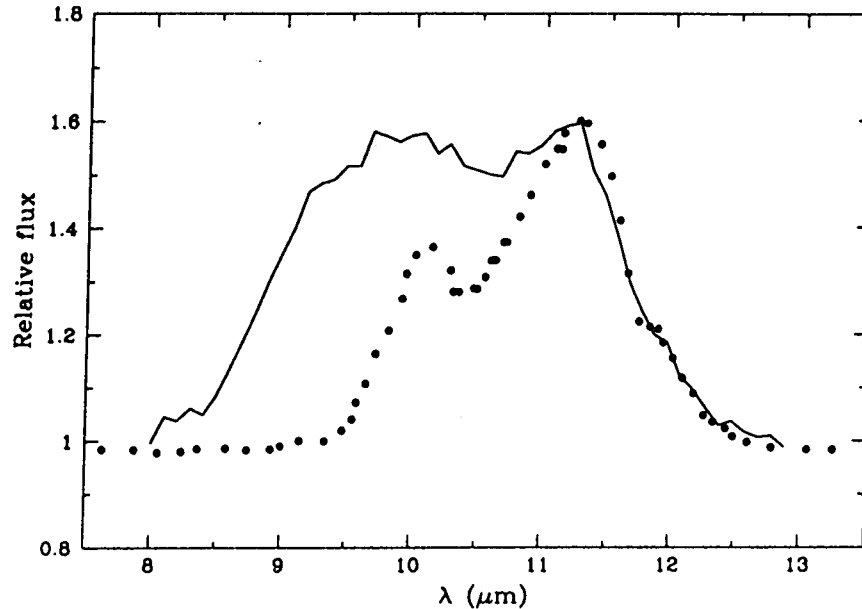


Figure 9. The 11.25  $\mu\text{m}$  feature of crystalline olivine. Filled circles: measured emissivity of ground olivine (Stephens & Russell 1979). Solid line: comet Halley flux/continuum (Campins & Ryan 1989). Figure from Hanner et al. (1994).

fitted at 8 and 12.5-13  $\mu\text{m}$ . Not only does the feature increase in strength relative to the continuum, but also the spectral structure becomes more prominent as the comet approaches perihelion. A broad peak emerges at 10.0  $\mu\text{m}$  and a definite shoulder appears at 9.2-9.3  $\mu\text{m}$ .

To demonstrate the reality of the spectral structure, we compare in Fig. 7 spectra taken near perihelion with 3 different instruments at 3 different sites. The 9.2  $\mu\text{m}$  bump is clearly separated from the noise introduced by the ozone absorption near 9.5  $\mu\text{m}$ . A small peak at 10.55  $\mu\text{m}$  is possibly present, especially in the HIFOGS spectrum.

Figure 8 compares the Hale-Bopp spectrum with a spectrum of P/Halley at 0.79 AU. The similarity of these spectra is striking. Spectra of Bradfield 1987 XXIX and Levy 1990 XX are similar (Hanner et al. 1994), including the inflection at 9.2  $\mu\text{m}$ . Since it represented only a single data point in those spectra however, the 9.2  $\mu\text{m}$  bump was never taken seriously.

### 3.2 SPECTRAL IDENTIFICATION

That the 11.2  $\mu\text{m}$  peak is due to crystalline olivine has been known since comet P/Halley (Bregman et al. 1987; Campins & Ryan 1989). A comparison of the Halley spectrum with the emissivity of a crystalline olivine sample is shown in Fig. 9. The 11.2  $\mu\text{m}$  peak is closely matched and even the small feature at 11.9  $\mu\text{m}$  is reproduced.

Dramatic confirmation of the olivine identification is revealed by the 6-45  $\mu\text{m}$  ISO SWS spectrum of Hale-Bopp at 2.9 AU, shown in Fig. 10.

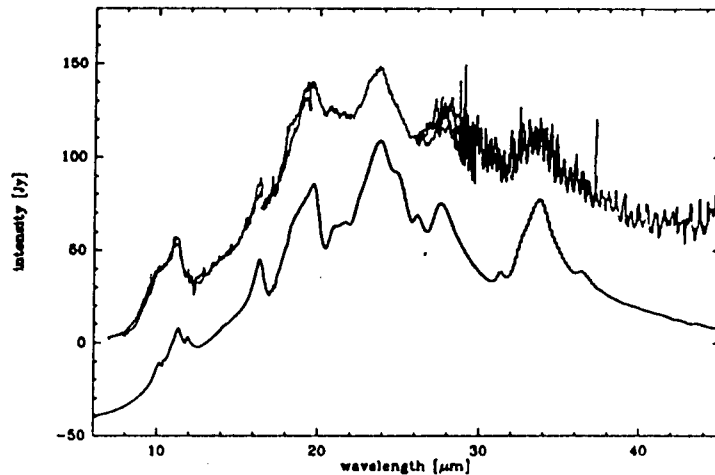


Figure 10. ISO SWS spectrum of Hale-Bopp October 6, 1996 (upper curve) and a modelled spectrum of forsterite (lower curve), (Crovisier et al. 1997b).

All of the major peaks in this spectrum correspond to peaks in the spectrum of Mg-rich crystalline olivine measured in the laboratory (Koike et al. 1993).

Now, the high signal/noise Hale-Bopp spectra allow us to interpret the rest of the 8-12  $\mu\text{m}$  feature.

Stephens & Russell (1979) measured the emissivity of ground (crystalline) and vapor-condensed (amorphous) Mg-rich samples of both pyroxene  $(\text{Mg,Fe})\text{SiO}_3$  and olivine  $(\text{Mg,Fe})_2\text{SiO}_4$ . Their emissivity for amorphous Mg-rich pyroxene is compared with the Hale-Bopp spectrum in Fig. 11. The amorphous pyroxene gives a good correspondence with the 9.2  $\mu\text{m}$  shoulder in the comet spectrum. Dorschner et al. (1995) have measured the optical constants for pyroxene glasses with a range of Mg/Fe content. The spectral peak occurs near 9.3  $\mu\text{m}$ , with some variation in peak wavelength with Fe content. Thus glassy or amorphous pyroxenes are a reasonable identification of the 9.2-9.3  $\mu\text{m}$  feature in the Hale-Bopp spectra.

Russell et al. (1997) have presented a model to fit the Hale-Bopp spectra by combining the 4 emissivities of amorphous and crystalline forsterite (Mg-olivine) and enstatite (Mg-pyroxene) measured by Stephens & Russell. They emphasized that these Mg-rich silicates should be the first to form in a cooling outflow around late-type stars.

Crystalline pyroxenes have considerable variety in their spectral shape. The orthorhombic orthoenstatite measured by Stephens & Russell has a narrow feature sharply peaked at 9.90  $\mu\text{m}$ . While orthoenstatite and clinoenstatite are found to exist together (Bradley et al. 1988), clinoenstatite is the most common form in IDPs (Bradley et al. 1992). These particles have a broader spectral feature, with the major peaks in the 10 - 11  $\mu\text{m}$  spectral region (Sandford & Walker 1985), and we propose that these pyroxenes provide a major contribution to the observed cometary spectra. Amorphous or glassy olivine produces a peak emissivity at 9.7-9.8  $\mu\text{m}$  and provides a reasonable match to the spectra of interstellar dust; it probably contributes to the 10  $\mu\text{m}$  cometary peak.

An example of a composite spectrum composed of 4 components -- amorphous and crystalline Mg-rich olivine and pyroxene -- is presented in Fig. 12. The transmission spectrum of "Key" IDP (Sandford & Walker 1985) was adopted for the crystalline pyroxene. Not only are the major spectral peaks accounted for, but also the overall width of the cometary feature is closely matched. Minor changes to the fit could be achieved by tweaking the relative proportions or by using a different IDP template; see Wooden et al. (1998a,b). The composite fit cannot be translated into relative abundances of the components, because the

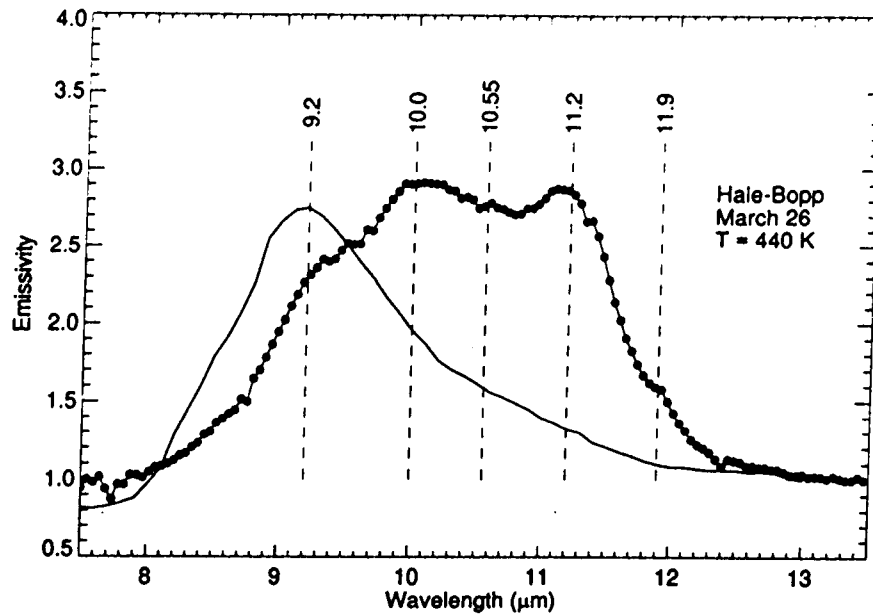


Figure 11. The emissivity of amorphous pyroxene compared with Hale-Bopp. Filled circles: SC10 spectrum of Hale-Bopp divided by 440 K blackbody; solid line: relative emissivity of amorphous Mg-pyroxene (Stephens & Russell 1979).

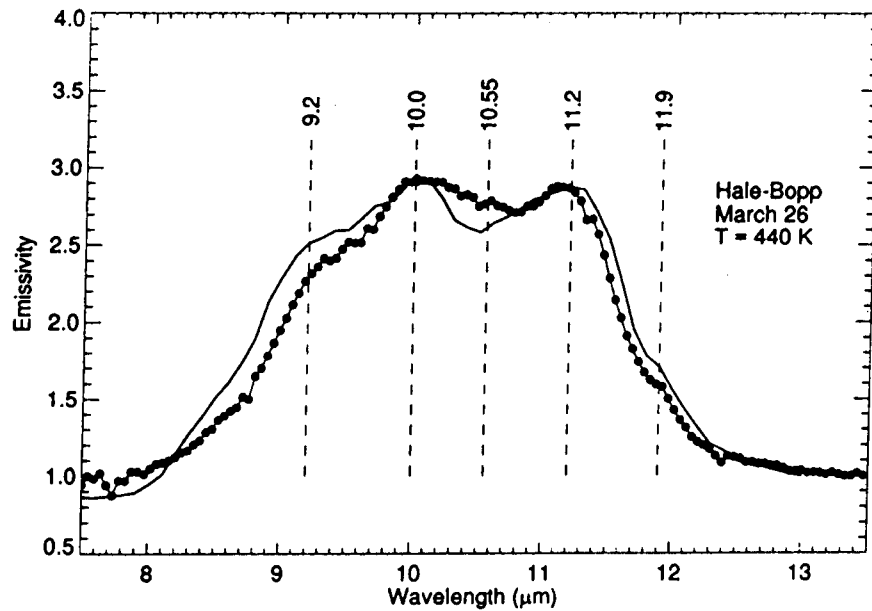


Figure 12. Composite spectral fit to Hale-Bopp silicate feature. Filled circles: SC10 spectrum of Hale-Bopp divided by 440 K blackbody; solid line: synthetic spectrum, consisting of emissivities for ground olivine, amorphous olivine, amorphous pyroxene (Stephens & Russell 1979) and "Key" pyroxene IDP (Sandford & Walker 1985).

absolute emissivities are not known. In general, crystalline silicates will have higher emissivity per unit mass than amorphous or glassy materials. Grain size and temperature also affect the emission.

This is not the first time such a composite mixture has been proposed (e.g. Bregman et al. 1987), but it is the first time that the cometary spectra have been of sufficient quality to make the fit convincing. We can confidently conclude that both olivine and pyroxene are present in cometary dust.

A detailed analysis of the spectral structure, emphasizing the role of crystalline pyroxene, is presented by Wooden et al. (1998a,b). They explain the changes in spectral shape with heliocentric distance by temperature differences between the pyroxene and olivine dust components. As we have shown in Fig. 2, the temperature of small silicate grains depends strongly on their transparency at visual wavelengths. Mg-rich pyroxenes have very low absorption (Dorschner et al. 1995). Consequently, their temperatures can be even cooler than the  $k=0.001$  curve in Fig. 2. Wooden et al. show that these cooler pyroxenes will contribute more strongly to the composite spectrum near perihelion, enhancing the strength of the 9.3, 10.0, and 10.5  $\mu\text{m}$  peaks. Galdemard et al. (1998) have also suggested temperature differences between olivine and pyroxenes to explain the Hale-Bopp spectra.

Wooden et al. also compute synthetic spectra for the full 8 - 45  $\mu\text{m}$  region covered by the SWS spectrum. They show that the contribution of pyroxenes is consistent with the shape of the spectral peaks in the SWS spectrum.

An alternate explanation for the structure in the 10  $\mu\text{m}$  silicate feature has been proposed by Hallenbeck et al. (1998). They measured the infrared spectra of initially amorphous silicate samples during annealing at  $T \sim 1000$  K. The spectra reached a "stall" at an intermediate stage of annealing, where a large amount of additional heating was required before the spectra evolved further. The stall spectra have bumps near 9.3, 10., and 11.1  $\mu\text{m}$ , somewhat resembling the comet spectra. Hallenbeck et al. suggest that silicates in astrophysical environments may reach the partially annealed "stall" stage and that comet grains may reflect such a process. However, the stall spectra do not display the sharp spectral features present in the 20  $\mu\text{m}$  Hale-Bopp spectrum. Nor are they consistent with the chondritic porous IDPs, in which fully crystalline silicate particles are common. While this mechanism may be applicable to some interstellar grains, it does not appear to describe the silicate grains in comets.

#### 4. Discussion

Were the grains in comet Hale-Bopp unique? Certainly, the extensive coma of refractory grains at large heliocentric distance, the unusually strong silicate feature, and the high color temperatures set Hale-Bopp apart from most other comets. However the dust composition, as revealed especially in the silicate features, appears to be typical of Oort Cloud comets, including P/Halley. In contrast, the size distribution was clearly weighted towards smaller (submicron) particles or very fluffy aggregates of such particles.

A major fraction of the interplanetary dust particles (IDPs) collected in the stratosphere for laboratory study are fine-grained heterogeneous aggregates having chondritic abundances of the major rock-forming elements. These chondritic aggregate IDPs divide into three classes dominated by pyroxenes, olivine, and layer lattice silicates, respectively (Sandford & Walker 1985; Bradley et al. 1992). The olivine and pyroxene rich IDPs are thought to originate from comets, based on their porous structure, high carbon content, and relatively high atmospheric entry velocities. Their composition is consistent with the elemental composition of the dust measured from the Halley flybys. It has been puzzling that the spectral signature of olivine was present in the cometary spectra, but that pyroxenes were not obvious. Now, it is clear from the Hale-Bopp spectra that pyroxenes are indeed present in the cometary dust, making the link between cometary dust and IDPs more secure. Thus, we can apply what has been learned about IDPs to enhance our understanding of cometary dust.

The pyroxene and olivine-rich IDPs are porous aggregates of glassy or microcrystalline silicate grains 0.1 to a few 0.1  $\mu\text{m}$  in diameter and larger single crystals of enstatite or olivine (0.5 - 5  $\mu\text{m}$  in size) along with carbonaceous material and FeS grains (Bradley et al. 1992). This aggregate structure suggests that differences in the size distribution among comets may be due to differences in the degree of aggregation of the grains. In Hale-Bopp, a larger fraction of the dust consists of single grains, whereas in comets with weaker silicate feature and temperatures closer to the equilibrium blackbody temperature, the grains are primarily aggregates.

Where did the cometary silicates form? Two clues from the IDPs point to an interstellar (IS) origin. (1) Enstatite whiskers and platelets up to 5  $\mu\text{m}$  long have growth patterns that indicate direct vapor phase condensation; these grains could not have formed by annealing (Bradley et al. 1983). (2) A common component of chondritic aggregate IDPs are 0.1-0.3  $\mu\text{m}$  diameter glassy silicate grains, or

GEMS (Glass with Embedded Metal and Sulfides). Bradley (1994) argues that these GEMS show evidence of a high radiation dose, such as eroded rims and metal beads, that could have occurred only in the IS environment.

Yet, observations of IS silicates, such as the Trapezium, show a smooth silicate feature with a single  $9.8\ \mu\text{m}$  maximum, very different from the cometary silicate feature. Most young stellar objects have silicate features consistent with the Trapezium (e.g. Hanner et al. 1998). However, the spectrum of the dust surrounding the young A5 V star  $\beta$  Pictoris resembles the comet spectra (Knacke et al. 1993). And HD100546, a late-stage Herbig AeBe star, has clear signatures of crystalline olivine in the ISO SWS spectrum (Waelkens et al. 1996; Waelkens 1998). Both of these systems are thought to have a population of comets, which are the source of the dust. Thus we have a circular argument, where comets seem to be necessary to produce the crystalline silicates, yet their dust appears to be pre-accretionary. Perhaps the on-going studies of both young and evolved stars with the ISO SWS will help to resolve these contradictions.

## 5. Conclusions

Hale-Bopp was a remarkable comet and the extensive infrared observations, over the entire wavelength range from 3 -  $160\ \mu\text{m}$  were remarkable as well. Observations at  $R=4.9\text{-}4.1$  AU from the ground and from ISO showed surprisingly high thermal emission at all wavelengths, a strong  $10\ \mu\text{m}$  silicate emission feature, and color temperatures  $\sim 30\%$  above an equilibrium blackbody, all indicative of small ( $< 1\ \mu\text{m}$  radius) silicate and absorbing grains. This contrasts to comet Bowell (1982 I), which apparently had a coma of large icy grains at 4-5 AU.

As the comet approached the sun, the contrast in the silicate feature increased and the  $3.5 - 5\ \mu\text{m}$  color temperature was almost a factor of two above the equilibrium blackbody temperature, both indicating that the mean grain size of the dust producing most of the emission at these wavelengths was, at most,  $1\ \mu\text{m}$  in diameter.

The most significant result from the infrared observations has been the mineralogical identification of the cometary silicates, based on the spectral structure in the  $8\text{-}13\ \mu\text{m}$  and  $16\text{-}35\ \mu\text{m}$  spectra. Both olivine and pyroxenes are present, linking the cometary dust to olivine-rich and pyroxene-rich chondritic aggregate IDPs, long thought to be of cometary origin. The cometary silicates are Mg-rich, consistent with the elemental composition of the dust measured during the Halley

flybys (Schulze et al. 1997). The pure Mg silicates, forsterite and enstatite are predicted from thermodynamic models to be the first to condense during slow cooling from the vapor phase in the atmospheres of evolved stars.

## **6. Acknowledgments**

Part of this work was carried out at the Jet Propulsion Laboratory, California Institute of Technology, under contract with the National Aeronautics and Space Administration. R.D.G. was supported by a grant from NASA.

## References

- A'Hearn, M.F., Schleicher, D.G., Feldman, P.D., Millis, R.L. and Thompson, D.T.: 1984, *Astron. J.* 89, 579-591.
- Bradley, J.P.: 1994, *Science* 265, 925-929.
- Bradley, J.P., Brownlee, D.E. and Veblen, D.R.: 1983, *Nature* 301, 473-477.
- Bradley, J.P., Humecki, H.J. and Germani, M.S.: 1992, *Astrophys. J.* 394, 643-651.
- Bradley, J.P., Sandford, S.A., & Walker, R.M. 1988, in *Meteorites and the Early Solar System*, ed. J.F. Kerridge and M.S. Matthews (Tucson: Univ. Arizona Press), p. 861.
- Bregman, J., Campins, H., Witteborn, F.C., Wooden, D.H., Rank, D.M., Allamandola, L.J., Cohen, M. and Tielens, A.G.G.M.: 1987, *Astron. Astrophys.* 187, 616-620.
- Campins, H. and Ryan, E.: 1989, *Astrophys. J.* 341, 1059-1066.
- Crovisier, J., Brooke, T.Y., Hanner, M.S., Keller, H.U., Lamy, P.L., Altieri, B., Bockelee-Morvan, D., Jorda, L., Leech, K. and Lellouch, E.: 1996, *Astron. Astrophys.* 315, L385-L388.
- Crovisier, J., Leech, K., Bockelee-Morvan, D., Brooke, T.Y., Hanner, M.S., Altieri, B., Keller, H.U. and Lellouch, E.: 1997, *Science* 297, 1904-1907.
- Davies et al. 1998, these proceedings.
- Davies, J.K., Roush, T.L., Cruikshank, D.P., Bartholomew, M.J., Geballe, T.R., Owen T. and de Bergh, C.: 1997, *Icarus* 127, 238-245.
- Dorschner, J., Begemann, B., Henning, Th., Jager, C. and Mutschke H.: 1995, *Astron. Astrophys.* 300, 503-520.
- Galdemard, P., Lagage, P.O., Pantin, E., Dubreuil, D., Jouan, R., Masse, P. and Bockelee-Morvan, D.: 1998, these proceedings.
- Gehrz, R.D. and Ney, E.P.: 1992, *Icarus* 100, 162.
- Greenberg, J.M. and Hage, J.I.: 1990, *Astrophys. J.* 361, 260-274.
- Grun, E. et al.: 1998, in preparation.
- Hallenbeck, S.L., Nuth, J.A. and Daukantas, P.L.: 1998, *Icarus*, 131, 198-209.
- Hanner, M.S.: 1983, in T.I. Gombosi (ed.) *Cometary Exploration*, Hungarian. Acad. Sci., Budapest, II, pp. 1-22.
- Hanner, M.S., Brooke, T.Y. and Tokunaga, A.T.: 1998, *Astrophys. J.*, in press.
- Hanner, M.S. and Campins, H.: 1986, *Icarus* 67, 51-62.
- Hanner, M.S., Lynch, D.K. and Russell, R.W.: 1994, *Astrophys. J.* 425, 274-285.

- Hanner, M.S. and Tokunaga, A.T.: 1991, in R.L. Newburn, M. Neugebauer, J. Rahe (eds.) *Comets in the Post-Halley Era*, Kluwer, Dordrecht, pp. 67-91.
- Hayward, T.L. and Hanner, M.S.: 1997, *Science* 275, 1907-1909.
- Hayward, T.L. and Hanner, M.S.: 1998, these proceedings.
- Khare, B.N., Sagan, C., Arakawa, E.T., Suits, F., Callcott, T.A., and Williams, M.W.: 1984, *Icarus* 60, 127-137.
- Knacke, R.F., Fajardo-Acosta, S.B., Telesco, C.M., Hackwell, J.A., Lynch, D.K., and Russell, R.W.: 1993, *Astrophys. J.* 418, 440.
- Koike, C. Shibai, H. and Tuchiyaama, A.: 1993; *Mon. Not. Roy. Astron. Soc.* 264, 654-658.
- Millis, R.L., A'Hearn, M.F. and Thompson, D.T.: 1982, *Astron. J.* 87, 1310.
- Peschke, S.B. et al.: 1998, these proceedings.
- Russell, R.W., Lynch, D.K., Mazuk, A.L., Rossano, G.S., Hanner, M.S. and Sitko, M.L.: 1997, *Bull. Amer. Astron. Soc.* 29, 1041.
- Sandford, S.A. and Walker, R.M.: 1985, *Astrophys. J.* 291, 838-851.
- Schulze, H., Kissel, J. and Jessberger, E.K.: 1997, in *From Stardust to Planetesimals*, ed. Y.J. Pendelton and A.G.G.M. Tielens, ASP Conf. Ser. 122 (Provo: ASP), p. 397.
- Stephens, J.R. and Russell, R.W.: 1979, *Astrophys. J.* 228, 780-786.
- Tokunaga, A.T., Golisch, W.F., Griep, D.M., Kaminski, C.D. and Hanner, M.S.: 1986, *Astron. J.* 92, 1183-1190.
- Waelkens, C.: 1998, these proceedings.
- Waelkens, C., et al.: 1996, *Astron. Astrophys.* 315, L245-L248.
- Williams, D.M., Mason, C.G., Gehr, R.D., Jones, T.J., Woodward, C.E., Harker, D.E., Hanner, M.S., Wooden, D.H., Witteborn, F.C. and Butner, H.M.: 1997, *Astrophys. J.* 489, L91-L94.
- Wooden, D.H., Harker, D.E. Woodward, C.E. and Butner, H.M.: 1997, *IAU Circ. No.* 6741.
- Wooden, D.H., Harker, D.E., Woodward, C.E., Butner, H.M., Koike, C. and Butner, H.M.: 1998a, these proceedings.
- Wooden, D.H., Harker, D.E., Woodward, C.E., Koike, C., Witteborn, F.C., and McMurtry, M.C.: Butner, H.M.: 1998b, *Astrophys. J.*, submitted.
- Xing, Zh. and Hanner, M.S.: 1997, *Astron. Astrophys.* 324, 805-820.